Modal Characteristics of Ferromagnetic Tridisk-Coupled Resonator

Tsukasa Nagao, *Senior Member, IEEE,* Zengo Tanaka, Hisashi Morishita, and Ikue Makita

Abstract— **The Eigenvalue characteristics of a ferrimagnetic tridisk-coupled (TDC) resonator are described first. A TDC resonator is made of three AlYIG ferrite disks partially scraped and mutually attached on a center conductor. The EM field is treated with a consistent theory. The eigenvalue characteristics computed with stress on the mode of ν=1 are represented by the Z_{10} versus Z_0 and Z_1 versus κ/μ relationships, where Z_{10} is a degenerate eigenvalue, Z_0 is a wavenumber-eccentric radius product, and Z_1 is a continuously varying eigenvalue dependent on κ/μ, with a given value of Z_0. Z_{10} is distinguished by either a single- or double-value region as a function of Z_0. The computed Z_1 versus κ/μ graph belonging to the double-value region demonstrates a contradiction to the physical reality, which is resolved by introducing an equivalent circular resonant mode. The equivalent resonant mode is definitely identified by a degenerate eigenvalue and its modal curve with large modal separation. Experiments were carried out with various center conductors. The experimental results support the equivalent resonant mode. Finally, discussions are presented.**

I. Introduction

THIS PAPER analytically treats an eigenvalue problem of a ferrimagnetic TDC resonator and its equivalent EM field representation, part of which was recently reported in [1] and [2]. In the TDC resonator, three ferrite disks were joined as shown in Fig. 1, and each of them was partially scraped. A treatise of such TDC resonator is found in [3], which analyzed cloverleaf planar resonators with the finite-element method, but none of experiments and related modal representations.

The analytical method adopted in this paper includes an accurate transformation of derivatives between the two coordinates systems $(\rho,\ \theta,\ z)$ and $(r,\ \phi,\ z)$, respectively, applied to a constituent disk and TDC resonator. If relevant transformations obey general rules of transformation in orthogonal curvilinear coordinates systems, the EM field equations, as it is known, hold invariant under transformation. Thus, the EM field confirmed in the TDC resonator satisfies the invariance under the transformation and the boundary condition of continuity. Contrastively speaking, the EM field shown in [2] is considered rather indefinite, since it lacks the invariance of form.

The computed eigenvalue characteristics are represented in two diagrams of the Z_{10} versus Z_0 and Z_1 versus κ/μ relationships. For the Z_{10} versus Z_0 diagram, there are single- and double-value regions, and for the Z_1 versus κ/μ diagram, it is found to contradict physical reality in that a Z_1 versus κ/μ graph belonging to the double-value region retains two degenerate eigenvalues. In connection with the double-value region, the wave behaviors possibly taking place inside the resonator are phenomenologically examined using a wave passage circumgyrating around three disks.

Manuscript received December 28, 1992; revised February 22, 1994.

The authors are with the Department of Communication Engineering, National Defense Academy, Kanagawa 239, Japan.

IEEE Log Number 9406810.

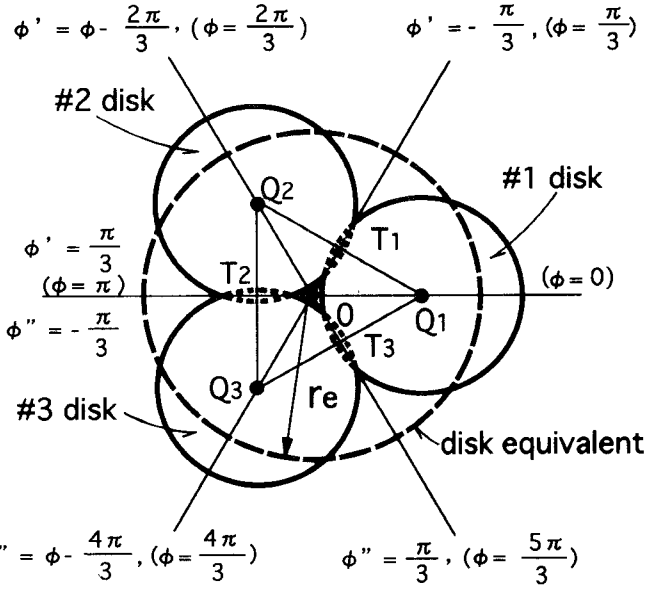

Fig. 1. Geometrical configuration of the TDC resonator and its disk equivalent and location of three disks and the connecting boundaries.

An equivalent circular cylindrical EM field representation is contrived to retain a given degenerate eigenvalue. The equivalent EM field representation aims to fix a circular disk of radius r_e and, furthermore, to confirm the equivalent resonant mode that displays unique modal separation.

The modal separations in the TDC resonator mode is described in comparison with that of a disk resonator. It is taken into account by the multiplier B_0, which is applied to κ/μ in calculating of resonant modal curves.

Experiments of TDC resonators with various center conductors were carried out. Modal behaviors in measured mode charts are found generally to agree with the above-noted equivalent resonant mode. Further discussions are given in relation to the fringing field effect.

II. Field Analysis of TDC Resonator

A. Preliminary Notes on Theoretical Treatment

To avoid a repetition of the mathematical procedure that was stated in [2], the present way of calculation is briefly noted

as follows. Utilizing the relevant transformation relations between the two coordinates systems that are given in Appendix A ((A8) and (A9)), one can prove that the EM field given in the system $(\rho,\ \theta,\ z)$ in [2, (7)–(9)] is invariantly transformed into that in the system $(r,\ \phi,\ z)$. For convenience, several radial wavenumber-radius products such as

$$w = k\rho, \qquad Z = kr, \qquad Z_0 = kr_0, \qquad Z_1 = ka, \tag{1}$$

are used hereafter. By making use of the transformation relations and the addition theorem of the Bessel functions [5], the EM field is described in the circular harmonic expansion as follows.

$$E_Z(Z,\ \phi) = \sum_\nu a_\nu \sum_m J_{\nu+m}(Z) J_m(Z_0) e^{-j(\nu+m)\phi}, \tag{2}$$

$$H_r = +\frac{1}{\zeta_e}\sum_\nu a_\nu \sum_m \left[\frac{(\nu+m)}{Z} J_{\nu+m}(Z) - \frac{\kappa}{\mu} J'_{\nu+m}(Z)\right] J_m(Z_0) e^{-j(\nu+m)\phi + j\Phi_\nu}, \tag{3}$$

$$H_\phi = -j\frac{1}{\zeta_e}\sum_\nu a_\nu \sum_m \left[J'_{\nu+m}(Z) - \frac{\kappa}{\mu}\frac{(\nu+m)}{Z} J_{\nu+m}(Z)\right] J_m(Z_0) \cdot e^{-j(\nu+m)\phi + j\Phi_\nu}, \tag{4}$$

where $\sum_\nu$ and $\sum_m$, respectively, denote $\sum_{\nu=-\infty}^{\infty}$ and $\sum_{\nu=-\infty}^{\infty}$, and J'_i denotes the derivative of the Bessel function of the first kind J_i. Thus, we can obtain the EM field of the first disk positioned at Q_1 $(\phi = 0)$. Further if we take $\phi' = \phi - 2\pi/3$ for the second disk in place of ϕ in (2), (3), and (4) and $\phi'' = \phi - 4\pi/3$ for the third disk, we can obtain the respective EM fields for the disks positioned at Q_2 $(\phi = 2\pi/3)$ and Q_3 $(\phi = 4\pi/3)$.

B. Continuity Conditions of Transverse EM Field Components

A TDC resonator is actually a juncture of three circular disks, and each disk contacts with others at $\phi = \pi/3$, π, and $5\pi/3$ as indicated by T_1, T_2, and T_3 in Fig. 1. When the juncture makes a unique resonator, then the EM field satisfies the continuity condition at each interconnecting boundary. It gives at T_1, for instance,

$$E_{z1}\left(Z_1, \frac{\pi}{3}\right) = E_{z2}\left(Z_1, -\frac{\pi}{3}\right),$$
$$\mu_{e1} H_1\left(Z_1, \frac{\pi}{3}\right) = \mu_{e2} H_2\left(Z_1, -\frac{\pi}{3}\right), \tag{5}$$

where suffices 1 and 2 denote the field components for the disk positioned at Q_1 and Q_2. Similar relations also hold at T_2 and T_3. $\mu_{e1} = \mu_{e2} = \mu_{e3}$ is assumed in calculation.

Algebraic manipulation of (5), after substitution of (2) and (4) and elimination of a_ν, gives the same complex characteristic equation for each of three boundaries T_1, T_2, and T_3 with respect to every ν $(-\infty < \nu < +\nu)$ as follows.

$$\left[\sum_m \left\{J'_{\nu+m}(Z_1) - \frac{\kappa}{\mu}\frac{(\nu+m)}{Z_1} J_{\nu+m}(Z_1)\right\} J_m(Z_0) \cdot e^{-jm\pi/3 + j\Phi_\nu}\right]\left[\sum_{m'} J_{\nu+m'}(Z_1) J_{m'}(Z_0) e^{jm'\pi/3}\right]$$
$$= \left[\sum_m \left\{J'_{\nu+m}(Z_1) - \frac{\kappa}{\mu}\frac{(\nu+m)}{Z_1} J_{\nu+m}(Z_1)\right\} J_m(Z_0) \cdot e^{+jm\pi/3 + j\Phi'_\nu}\right]\left[\sum_{m'} J_{\nu+m'}(Z_1) J_{m'}(Z_0) e^{-jm'\pi/3}\right] \tag{6}$$

In order to obtain a physically significant value from this characteristic equation, the real part of (6) should be retained under the phase condition

$$\Phi'_\nu = \pi - \Phi_\nu. \tag{7}$$

We deduce from (6), after substitution of (7),

$$\sum_m \sum_{m'} \left[J'_{\nu+m}(Z_1) - \frac{\kappa}{\mu}\frac{(\nu+m)}{Z_1} J_{\nu+m}(Z_1)\right] \cdot J_{\nu+m'}(Z_1) J_m(Z_0) J_{m'}(Z_0) \cos\{(m-m') \cdot \pi/3 - \Phi_\nu\} = 0, \qquad m,\ m' = 0,\ \pm 1,\ \pm 2, \cdots \tag{8}$$

Choice of $\Phi_\nu = 0$ is needed.

C. Eigenvalue Characteristics of TDC Resonator

Computation of (8) is made, at first, to get a degenerate eigenvalue Z_{10} $(= [ka])$ with $\kappa/\mu = 0$, and next to get an eigenvalue Z_1 $(= ka)$ as a function of κ/μ, regarding $\nu = 1$ and 2 in addition. Computed results of two kinds of the eigenvalues are shown in Figs. 2 and 3. To explain the

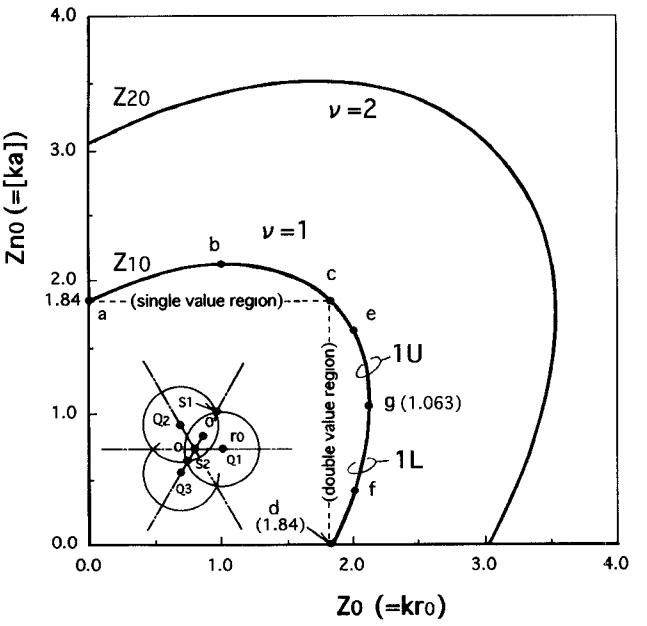

Fig. 2. The Z_{10} versus Z_0 diagram and the relationship of Z_{10} and Z_{20}. m and m' in computation of (8) are retained to 12. Inset is geometrical configuration of a pair disk in the TDC resonator.

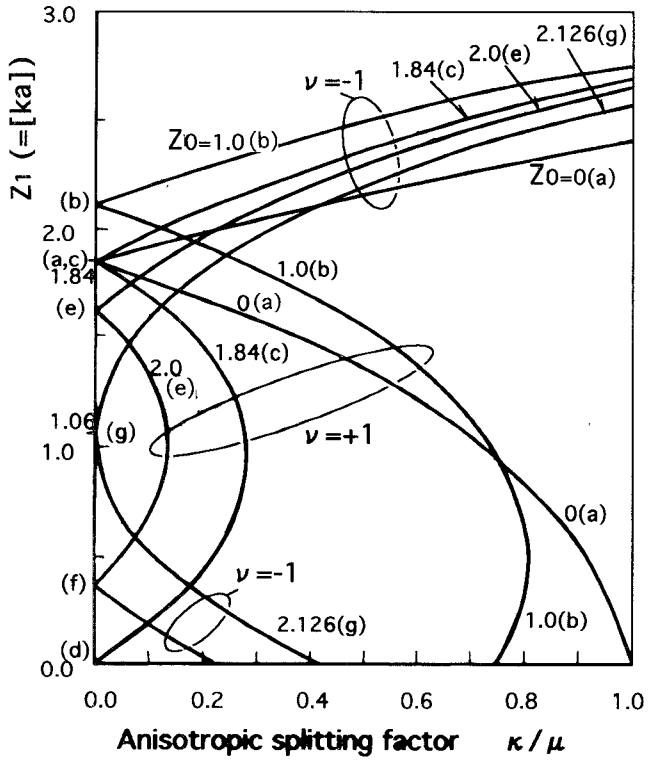

Fig. 3. The Z_1 versus κ/μ diagram. m and m' in computation of (8) are retained to 12. Notations a, b, and others in parentheses are referred to those in Fig. 2.

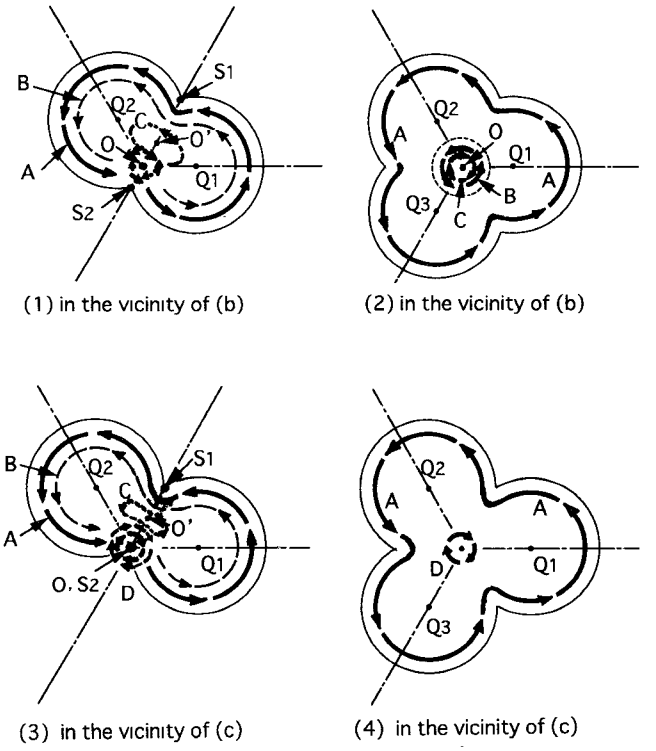

Fig. 4. Illustration of wave passages circumgyrating in the positive direction in a pair disk and a TDC resonator in the vicinity of (b) and (c).

characteristics of Z_{10}, we put marks from a to g on these diagrams. The Z_{10} versus Z_0 diagram demonstrates that as Z_0 and, of course, the radius of eccentricity r_0 increases from zero, Z_{10} increases slightly from 1.84 (a), and after it reaches the maximum $Z_{10} = 2.12$ (b) at $Z_0 = 1.06$, it decreases to $Z_{10} = 1.84$ (c) at $Z_0 = 1.84$; beyond (c), it occurs to have double values, for instance, (c) and (d) or (e) and (f), denoted by $1U$ and $1L$, respectively. The Z_{20} versus Z_0 diagram for $\nu = 2$ is additionally drawn in Fig. 2. It totally resembles that of $\nu = 1$.

The Z_1 versus κ/μ diagram with a variety of Z_{10} is summarized as follows: 1) The graph marked by (a) has the same variation in κ/μ as the resonant modal curve of a disk resonator since the $\nu = +1$ curve runs from the degenerate point where $Z_1 = 1.84$ and $\kappa/\mu = 0$ to the cutoff point where $Z_1 = 0$ and $\kappa/\mu = 1.0$; 2) A change from (a) to (b) is an increase of Z_{10} from 1.84 to 2.12. The graph marked by (b) is almost similar to that of (a), but the pair of the graphs are more separated, with the cutoff point moved to $\kappa/\mu = 0.74$ from 1.0. Another change to (c) is a decrease of Z_{10} to 1.84, with larger separation, and simultaneously it occurs to have an extra of $Z_{10} = 0$ (d), with the cutoff point moved from $\kappa/\mu = 0.74$ to 0; 3) In the double-value region, a graph is traced in a line passing two points, (e) and (f), for instance, with its sign changed from minus to plus at (e) and vice versa at (f). If Z_0 increases still further, they finally join at (g) where $Z_{10} = 1.06$ and $Z_0 = 2.12$ and the TDC resonator collapses into the constituent disk resonators.

The wave behaviors possibly taking place in the TDC resonator can be examined phenomenologically by using wave passages circumgyrating around the three disks, with regard to (b) and (c) on the Z_{10} versus Z_0 diagram. Assume that the wave passage in the TDC resonator may be decomposed into such elemental wave passages in each pair of the disks, as shown in Fig. 4. The geometry of the pair disk is shown inset in Fig. 2. In the case of (b) with $Z_0 = 1.06$ where the center O situates between O' and S_2, two waves, A and C, respectively, pass through between S_2 and O and between O and O' in the same direction as shown in Fig. 4(a). When they are transferred to around O in the resonator, they counteract each other to be void of them in the central part, as shown in Fig. 4(b). In the case of (c) with $Z_{10} = Z_0 = 1.84$ where O coincides with S_2, the waves A, B, and C passing between O and O' in the pair disk produce the major wave A circumgyrating and the minor wave D inversely rotating in the resonator, as shown in Fig. 4(c) and (d). Thus, two degenerate points of (c) and (d), and (e) and (f) occur as well.

III. Equivalent Circular Cylindrical Wave Representation of the EM Field

A. Synthesis of Equivalent Circular Cylindrical EM Field

It should be noted that any of the Z_1 versus κ/μ graphs that have been shown in Fig. 3 are not precisely of circular cylindrical waves, since the EM field given by (2)–(4) is still in the form of the expanded harmonic wave; besides, some of the graphs retain two degenerate eigenvalues. As far as a ferrimagnetic resonator is concerned, one degenerate eigenvalue definitely determines one unique resonant mode. It is necessary to derive a circular cylindrical wave expression that consists of each one of the above-noted degenerate eigenvalues. Deriva-

tion of the circular EM field can be made by synthesis from the constituent EM fields as noted in [2]. We assume that the TDC resonator has an equivalent circular disk of radius r_e and the corresponding anisotropic splitting factor $(\kappa/\mu)'$, and subsequently the EM field effectively satisfy the boundary condition of the magnetic wall. The EM field is obtained, by summation, from the constituent EM fields according to three cases: zero-phase, positive-phase, and negative-phase junctures. Summarizing thus-synthesized EM fields, we can describe the EM fields of all modes of n as follows.

$$E_z = \sum_n a_n J_n(Z) e^{-jn\phi}, \tag{9}$$

$$H_r = +\frac{1}{\zeta_e}\sum_n a_n \left[\frac{n}{Z} J_n(Z) - (\kappa/\mu)' J_n'(Z)\right] e^{-jn\phi}, \tag{10}$$

$$H_\phi = -j\frac{1}{\zeta_e}\sum_n a_n \left[J_n'(Z) - (\kappa/\mu)' \frac{n}{Z} J_n(Z)\right] e^{-jn\phi}, \tag{11}$$

Now, we have for the magnetic wall condition, $H_\phi = 0$, from (11)

$$J_n'(Z_2) \mp (\kappa/\mu)' \frac{1}{Z_2} J_1(Z_2) = 0, \tag{12}$$

where

$$Z_2 = kr_e, \qquad (\kappa/\mu)' = B_0 \kappa/\mu, \tag{13}$$

and B_0 is a multiplier.

B. Adjustment of Resonant Modal Curves with Disk Equivalent

The EM field given by (9)–(11) resumes the circular cylindrical wave expression, but (12) does not yet retain any of the above-described degenerate eigenvalues. To meet the requirement that the EM field is to consist with a given value of Z_{10} and to sustain a presupposed gradient angle of a Z_1 versus κ/μ graph, some prerequisites are necessary to describe lowering of a degenerate eigenvalue and adjustment of its modal gradient angle. As we know, the degenerate eigenvalue computed from (12) is none other than the one of the disk resonator for $\nu = 1$, and we have for this mode

$$Z_2 = kr_e = 1.84. \tag{14}$$

The aim is that the equivalent resonant modal curves with a given degenerate eigenvalue $Z_{10} \gtreqless 1.84$ can be reproduced from those of the disk resonator by adjusting r_e and B_o in (13).

Equivalent radius for given degenerate eigenvalue: For an instance of $Z_{10} < 1.84$, as the radius r_e of the disk equivalent may be larger, so it is written as

$$r_e = a(1 + \Delta), \tag{15}$$

where Δ is a radius increment. Decreasing of Z_{10} from 1.84 may be ascribed to such increment. After substitution of (15) into (14), one can obtain

$$kr_e = [ka](1 + \Delta) = 1.84.$$

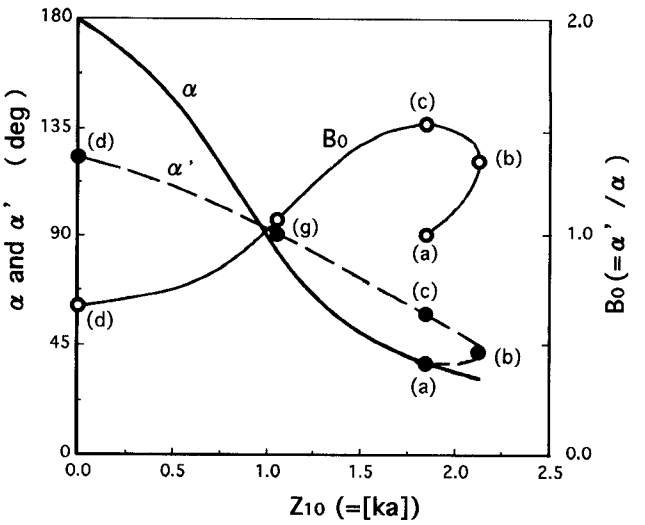

Fig. 5. Relationship of initial gradient angles α and α' against Z_{10} and relationship of B_0 against Z_{10}. Notations (a)–(g) correspond to those in Figs. 2 and 3.

Thus, $[ka]$ of the present interest is evaluated as

$$Z_{10} = [ka] = 1.84/(1 + \Delta), \tag{16}$$

and the radius r_e becomes

$$r_e = 1.84\ a/[ka]. \tag{17}$$

Consequently, we can obtain for an arbitrary value of ka with the degenerate eigenvalue $[ka]$

$$Z_2 = kr_e = 1.84\ ka/[ka]. \tag{18}$$

Modal separation and multiplier: A pair curve of a resonant mode in a disk resonator is intrinsically separated under the biasing magnetic field. This separation is described by an initial gradient angle α_1 of a tangential straight line passing a degenerate point Z_{10} as given in Appendix C. The initial angle for the mode of $n = 1$ is given by

$$\alpha_1 = \cot^{-1}(Z_{10} - 1/Z_{10}). \tag{19}$$

The angle α_1 computed from (19) and the theoretical angle α_1' obtained from the curves of Fig. 3 are shown in Fig. 5. α_1 simply varies from 38° to 180° if Z_{10} decreases from 1.84 to zero, while α_1' varies from 38° to 120°. α_1' is equal to α_1 at $Z_{10} = 0.97$.

The ratio of gradient angles is preferred to in definition of B_0

$$B_0 = \alpha_1'/\alpha_1, \tag{20}$$

and it is shown in Fig. 5. B_0 is more than unity in the range above $Z_{10} = 0.97$ and less below it. B_0 is related to the cutoff value of $(\kappa/\mu)_c$, as given by

$$B_0 = 1/(\kappa/\mu)_c. \tag{21}$$

Thus, the shifting of the cutoff value on the axis of κ/μ is related to the modal separation. B_0 is also understood to represent an enhancement of κ/μ due to gaining more phase angle than 2π by circumgyrating the peripheral passage.

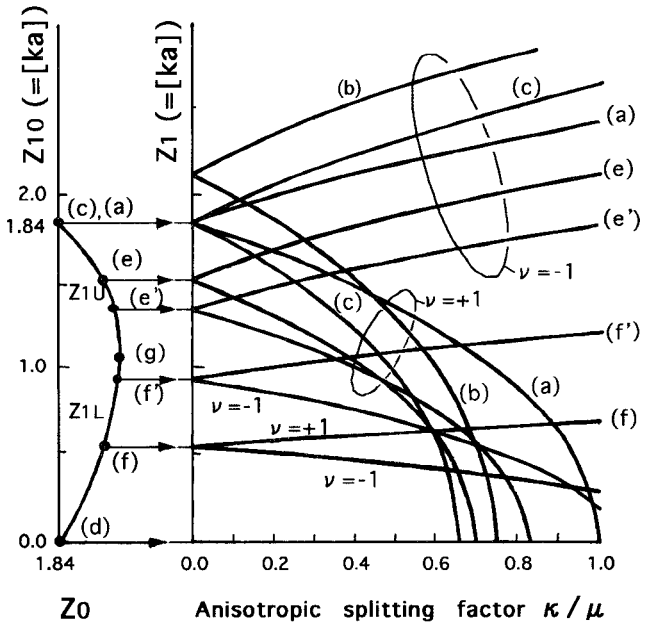

Fig. 6. Equivalent resonant modal curves. Part of the Z_{10} versus Z_0 diagram in the left side is transferred from Fig. 2.

Graphing of resonant modal curves: Computation of (12) is made taking into account the $[ka]$ and B_0 relation shown in Fig. 5. The computed results of the resonant modal curves are shown in Fig. 6, where (a), (b), and others correspond to those in Figs. 2 and 3. The resonant modal curves obviously get more separated if their value of Z_0 varies from (a) through (b) to (c) and the cutoff point of $(\kappa/\mu)_c$ moves down and back from $\kappa/\mu = 1.0$ to 0.64. In contrast, the separation for $1L$ becomes smaller than for $1U$ and the curves of $1L$ have no cutoff, running almost straight on a level with its degenerate point. To ascertain the above graphing, we need some evidence to rely on.

IV. Experiments and Discussions

The TDC resonator used in experiment had such specifications that the radius of a disk was $a = 10$ mm, its thickness was 2.5 mm, scraped depth was 1.0 mm, saturation magnetization of AlYIG ferrite $4\pi M_s = 950$ Gauss, and its permittivity was $\epsilon_e = 14.5$. Since the radius r_0 was 10.4 mm, which was less than 11.55 mm for a resonator with nothing scraped, the resonator of the present concern belonged to the double-value region near $Z_0 = 1.84$. Resonators having a narrow stripline for light coupling and a wide stripline for tight coupling, with various center conductors, were experimented.

A lightly coupled resonator was made of a center conductor of type 1 and coupled by use of the narrow stripline of width $W = 4$ mm. The resonant frequency curves measured in the above resonance were found to be the same narrowly separated pair as seen in a mode chart in [2, Fig. 7]. It is considered to be a pair of $1L$.

In the tightly coupled cases, the resonators, at first, had only common circular center conductors (type 2), so that three ferrite disks partially protruded out of the center conductor, and later had such protruded portions backed with conductors besides the circular center parts (type 3). The type-2 conductor

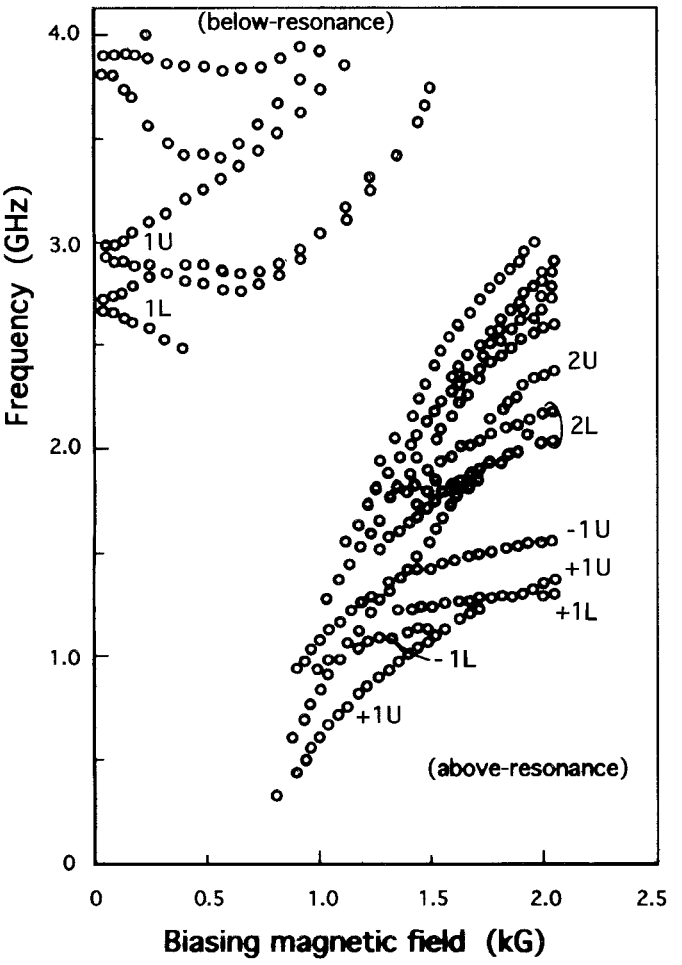

Fig. 7. Measured mode chart of tightly coupled resonator with a type-2 center conductor of diameter $2r_e = 33$ mm. Coupled stripline width $W = 11.2$ mm.

had the center conductor of $2r_e = 33$ mm and coupled striplines of width $W = 11.2$ mm. An obtained mode chart is shown in Fig. 7. Resonant frequency curves of $n = 1$ were distinguished by two pairs of $1U$ and $1L$ in the above and below resonance. In the above resonance, the $1L$ curves showed the feature to lie between two curves of $1U$ in the biasing magnetic field near 1.5-kilo Gauss and a tendency to depart from $1U$ as the magnetic field increased. This observation corresponds to the relationships of $1U$ and $1L$, which are respectively marked by (e) and (f) in Fig. 6.

Further experiments were carried out using larger center conductors of types 2 and 3. One typical mode chart measured with a type-3 conductor is shown in Fig. 8. Two pairs of resonant frequency curves of $1U$ and $1L$ are narrowly separated and decisively departed from each other.

A resonant frequency at a degenerate point, named degenerate resonant frequency (DRF), is estimated by extrapolation at the extremity of biasing magnetic field. DRF's of $1U$ and $1L$ in the above and below resonance for all coupling cases and conductor types are plotted in Fig. 9. Those of the lightly coupled case are plotted at $2r_e = 19$ mm since the type-1 conductor has the inscribed circle of $r_e = 9.5$ mm, while those with the type-2 and 3 conductors for such as shown in Fig. 7 are plotted at $2r_e = 33$ mm, though the DRF's of

TABLE I
THEORETICAL DIAMETERS OF DISK EQUIVALENTS

No.	Z_0	$[ka]_{1U}$	$[ka]_{1L}$	Mean Value	Diameter $2r_e$ (units: mm) for a = 20;	for a = 18
1	1.90	1.77	0.13	0.95	38.7	34.9
2	2.00	1.63	0.37	1.00	36.8	33.1
3	2.50	1.33	0.75	1.04	35.5	31.8

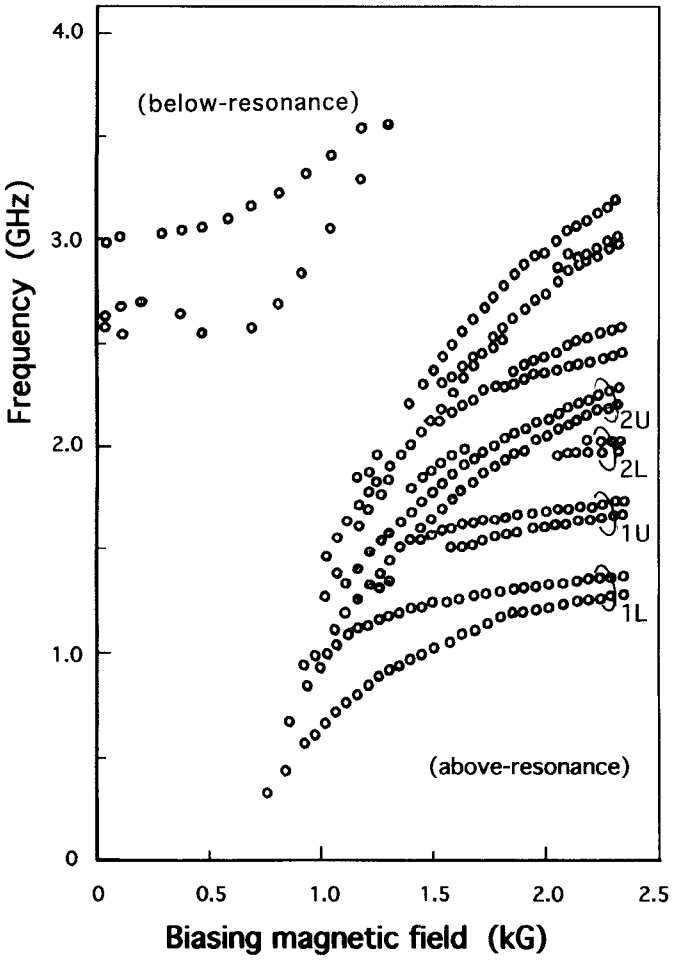

Fig. 8. Measured mode chart of tightly coupled resonator with a type-3 center conductor of $2r_e = 36.5$ mm. Coupled stripline width: $W = 11.2$ mm.

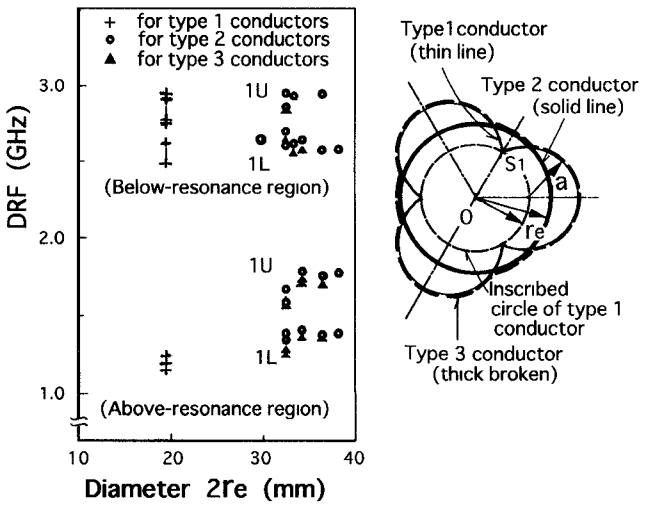

Fig. 9. Relationship of degenerate resonant frequencies of $1U$ and $1L$ against disk diameters of various center conductors in the above- and below-resonance regions.

the type-2 conductor are slightly higher. When the conductor diameter exceeds $2r_e = 35$ mm, DRF's of $1U$ and $1L$ for such performance as shown in Fig. 8 are found almost unchanged.

Thus, the existence of the double resonant modes of $1U$ and $1L$ as shown in Figs. 7–9 verifies the theoretical prediction of the two modes. Regarding the double resonant modes of $1U$ and $1L$, there is an adequate center conductor radius to consolidate them. A disk equivalent to this end is calculated from the mean value of two degenerate eigenvalues for $1U$ and $1L$. Using (17), one can calculate diameters for some disk equivalents as follows.

Comparing the diameters experimentally examined as shown in Fig. 9 and those calculated as given in Table I, we find that the experimental diameter $2r_e = 33$ mm is shorter than any one for $a = 20$ mm. If we assume $a = 18$ mm, we have $2r_e = 33.1$ mm for $Z_0 = 2.00$, which agrees with the experimental diameter noted above.

Qualitative reasoning about the diametric discrepancy is sought from the view point of the fringing field effect [6]–[8]. It is actually unavoidable that when a uniform biasing magnetic field is applied, the internal magnetic field is not wholly uniform in the ferrite disk and becomes oblique in the fringe of the disk. Accordingly, inhomogeneity of dispersive and dissipative components of the tensor magnetic permeability is brought about in the fringe in the above and below resonance regions [8], [9]. The resonance condition of the magnetic wall and the loss factor may be seriously affected. Thus, the boundary surface is physically modified to move back inside the disk, so that the diameter and the scraped portion are in effect reduced. The diameter reduction from $a = 20$ to 18 mm results in increasing Z_0 and correspondingly brings two degenerate eigenvalues closer in the Z_{10} versus Z_0 diagram. Thus, the calculated diameter of the disk equivalent supports the above reasoning.

The dispersive and dissipative components inhomogeneously emerging in the fringe of the disk not only shift the boundary surface of the magnetic wall, but also affect the Q factor of the resonator and its impedance matching, so that measurement of resonant frequency is seriously influenced. Missing resonant frequencies seen in a mode

chart are considered mostly caused by low SN ratio, due to the dissipation in the fringe in addition to the inhomogeneous dispersive component.

V. Conclusion

The boundary value problem of the TDC resonator and the eigenvalue characteristics are treated with stress on the lowest-order mode. As for the Z_{10} versus Z_0 diagram, there are single- and double-value regions, part of which is phenomenologically examined using wave passages circumgyrating in the three ferrite disks in the resonator. As for the Z_1 versus κ/μ diagram, to dissolve the discrepancy between the theoretically computed curves and related resonant frequency curves drawn in the mode chart, an equivalent circular resonant mode is contrived that is definitely to retain one degenerate eigenvalue. The TDC resonators with various center conductors were experimented and adequate center conductors were found necessary to consolidate the equivalent resonant mode.

It is finally noted that the resonant mode in the TDC resonator has potentiality to display larger modal separation and an enhancement effect of the anisotropic splitting factor due to such TDC structure. Application of a multidisk-coupled structure has been undertaken to extend performances of such nonreciprocal devices as isolator and circulator in VHF and EHF and to further realize such devices in the near infrared region.

VI. Appendix A
Transformation of Derivatives $\partial/\partial w$ and $\partial/w\,\partial\theta$

Transformation of the derivatives can be achieved according to the theory of differential geometry. One can assume the functions $w = f_1(Z, \phi)$, $\theta = f_2(Z, \phi)$, $Z = f_3(w, \theta)$, and $\phi = f_4(w, \theta)$ along the constant lines of w, θ, Z, and ϕ, referring to [2, (1)–(6)]. The issue can be restricted within two infinitesimal coordinates systems $(dw,\ wd\theta)$ and $(dZ,\ Zd\phi)$, which are mutually dependent on the direction cosines $(\lambda_1,\ \mu_1)$ and $(\lambda_2,\ \mu_2)$ between the two coordinates systems. They are given by

$$\lambda_1 = \frac{1}{h_1}\frac{\partial Z}{\partial w} = \frac{1}{g_1}\frac{\partial w}{\partial Z}, \qquad \mu_1 = \frac{1}{h_1}\frac{\partial Z}{w\partial\theta} = \frac{1}{g_1}\frac{w\partial\theta}{\partial Z},$$

$$\lambda_2 = \frac{1}{h_2}\frac{Z\partial\phi}{\partial w} = \frac{1}{g_2}\frac{\partial w}{Z\partial\phi}, \qquad \mu_2 = \frac{1}{h_2}\frac{Z\partial\phi}{w\partial\theta} = \frac{1}{g_2}\frac{w\partial\theta}{Z\partial\phi}. \tag{A1}$$

h_1, h_2, g_1, and g_2 in (A1) are the scale factors given by

$$h_1 = \sqrt{\left(\frac{\partial Z}{\partial w}\right)^2 + \left(\frac{\partial Z}{w\partial\theta}\right)^2}, \qquad g_1 = \sqrt{\left(\frac{\partial w}{\partial Z}\right)^2 + \left(\frac{w\partial\theta}{\partial Z}\right)^2},$$

$$h_2 = sqrt\left(\frac{Z\partial\phi}{\partial w}\right)^2 + \left(\frac{Z\partial\phi}{w\partial\theta}\right)^2, \qquad g_2 = \sqrt{\left(\frac{\partial w}{Z\partial\phi}\right)^2 + \left(\frac{w\partial\theta}{Z\partial\phi}\right)^2}, \tag{A2}$$

and they must satisfy the relations

$$g_1h_1 = 1, \qquad g_2h_2 = 1, \qquad \lambda_1\mu_2 + \mu_1\lambda_2 = 0. \tag{A3}$$

Now, let f be an arbitrary function of w, θ, Z, and ϕ, and the derivatives are calculated as

$$\frac{\partial f}{\partial w} = h_1\lambda_1\frac{\partial f}{\partial Z} + h_2\lambda_2\frac{\partial f}{Z\partial\phi}, \qquad \frac{\partial f}{w\partial\theta} = h_1\mu_1\frac{\partial f}{\partial Z} + h_2\mu_2\frac{\partial f}{Z\partial\phi}. \tag{A4}$$

All terms in the right side in (A1) and (A2) are calculated from the above-given functions f_1, f_2, f_3, and f_4. One can obtain

$$\frac{\partial w}{\partial Z} = \cos\psi = \frac{\partial Z}{\partial w}, \qquad \frac{w\partial\theta}{\partial Z} = -\sin\psi = \frac{\partial Z}{w\partial\theta},$$

$$\frac{\partial w}{Z\partial\phi} = \sin\psi = \frac{Z\partial\phi}{\partial w}, \qquad \frac{w\partial\theta}{Z\partial\phi} = \cos\psi = \frac{Z\partial\phi}{w\partial\theta}. \tag{A5}$$

Substituting (A5) into (A1) and (A2), one finds that as for the scale factors $h_1 = h_2 = 1$ and $g_1 = g_2 = 1$ and for the direction cosines

$$\lambda_1 = \cos\psi, \qquad \lambda_2 = \sin\psi, \qquad \mu_1 = -\sin\psi, \qquad \mu_2 = \cos\psi. \tag{A6}$$

Consequently (A4) is rewritten as

$$\frac{\partial f}{\partial w} = \cos\psi\frac{\partial f}{\partial Z} + \sin\psi\frac{\partial f}{Z\partial\phi}, \qquad \frac{\partial f}{w\partial\theta} = -\sin\psi\frac{\partial f}{\partial Z} + \cos\psi\frac{\partial f}{Z\partial\phi}. \tag{A7}$$

Transformation of magnetic field components H_ρ and H_θ into H_r and H_ϕ is made according to the relation

$$H_\rho = \cos\psi H_r - \sin\psi H_\phi, \qquad H_\theta = \sin\psi H_r + \cos\psi H_\phi. \tag{A8}$$

VII. Appendix B
Modal Separation of the n-th Order Mode at the Degenerate Point

Resonant modal curves of the n-th order mode are computed from the characteristic equation

$$J_n'(Z_n) \mp \frac{\kappa}{\mu}\frac{n}{Z_n}J_n(Z_n) = 0. \tag{B1}$$

The resonant modal curves drawn in the Z_n versus κ/μ diagram is approximated by a tangential straight line passing the degenerate point Z_{n0} with the gradient angle α_n. The degenerate point is given by the lowest root of

$$J_n'(Z_{n0}) = 0. \tag{B2}$$

Substituting into (B1) the approximate linear formulae of the Bessel function of the n-th order and its derivative which are given by $J_n(Z_n) = J_n(Z_{n0}) + J_n'(Z_{n0})\Delta Z_n$ and $J_n'(Z_n) =$

$J_n'(Z_{n0}) + J_n''(Z_{n0})\Delta Z_n$ regarding $Z_n = Z_{n0} + \Delta Z_n$, and taking the linear terms in the Taylor expansions of (B1), one can obtain for the gradient of the tangential line

$$dZ_n/d(\kappa/\mu) = -\frac{n}{Z_{n0}[1-(n/Z_{n0})^2]}. \tag{B3}$$

From (B3) one can obtain the gradient angle α_n

$$\alpha_n = \tan^{-1}\left[\frac{n}{Z_{n0}\{1-(n/Z_{n0})^2\}}\right]. \tag{B4}$$

REFERENCES

[1] T. Nagao and Z. Tanaka, "Magnetically tunable stripline Y circulator," *1990 IEEE MTT-S Int. Microwave Symp. Dig.*, CC-3, pp. 1011–1014, May 1990.

[2] T. Nagao and Z. Tanaka, "Ferromagnetic tridisk-coupled resonator and magnetically tunable stripline Y circulator," *IEEE Trans. Microwave Theory Tech.*, vol. MTT-40, no. 9, pp. 1812–1820, Sept. 1992.

[3] J. Helszajn and D. J. Lynch, "Cutoff space of cloverleaf resonators with electric and magnetic walls," *IEEE Trans. Microwave Theory Tech.*, vol. MTT-40, no. 8, pp. 1620–1629, Aug. 1992.

[4] T. Nagao and Z. Tanaka, "Diplexer operation of stripline Y circulator: Part 1," *IEEE Trans. Microwave Theory Tech.*, vol. MTT-28, pp. 776–786, July 1980.

[5] G. N. Watson, A Treatise on The Theory of Bessel Functions. 2nd ed. Cambridge University Press: Cambridge,, UK 1966.

[6] J. Eshbach, "Spin-wave propagation and the magnetoelastic interaction in Yttrium Iron Garnet," *J. Appl. Phys.*, Part 2, vol. 34, no. 4, pp. 1298–1304, Apr. 1963.

[7] R. Joseph and E. Schloemann, "Demagnetizing field in nonellipsoidal bodies," *J. Appl. Phys.*, vol. 36, no. 5, pp. 1579–1593, May 1963.

[8] E. Schloemann and R. Blight, "Broad-band stripline circulators based on YIG and Li-ferrite single crystals," *IEEE Trans. Microwave Theory Tech.*, vol. MTT-34, no. 12, pp. 1394–1400, Dec. 1986.

[9] B. Lax and K. Button, *Microwave Ferrites and Ferrimagnetics.* New York: McGraw-Hill, 1962, p. 151.

Tsukasa Nagao, photograph and biography not available at the time of publication.

Zengo Tanaka, photograph and biography not available at the time of publication.

Hisashi Morishita, photograph and biography not available at the time of publication.

Ikue Makita, photograph and biography not available at the time of publication.